

# Theoretical investigation on phosphorescent platinum complexes based on two tetradentate bipyridine ligands

Hadj MEZOUAR

University of Saida - Dr Moulay Tahar

Houari BRAHIM

[brahim.h@outlook.com](mailto:brahim.h@outlook.com)

University of Saida - Dr Moulay Tahar

Mostefa BOUMEDIENE

University of Tiaret – Ibn Khaldoun

Fatima YAHIA CHERIF

University of Saida - Dr Moulay Tahar

Djebar HADJI

University of Saida - Dr Moulay Tahar

Abdelkrim GUENDOZI

University of Saida - Dr Moulay Tahar


---

## Research Article

**Keywords:** TD-DFT, platinum, complexes, absorption, phosphorescence

**Posted Date:** February 6th, 2024

**DOI:** <https://doi.org/10.21203/rs.3.rs-3921913/v1>

**License:**   This work is licensed under a Creative Commons Attribution 4.0 International License. [Read Full License](#)

**Additional Declarations:** No competing interests reported.

---

**Version of Record:** A version of this preprint was published at Theoretical Chemistry Accounts on March 25th, 2024. See the published version at <https://doi.org/10.1007/s00214-024-03107-y>.

## Abstract

In this work, the geometrical, optical, and phosphorescence properties of four complexes with general formula  $[dRppy-C(OCH_3)R'-dRppy]Pt$ , with **Pt-1** (R = F, R'=methyl), **Pt-2** (R = F, R'=hexyl), **Pt-3** (R = methoxy, R'=methyl) and **Pt-4** (R = methoxy, R'=hexyl) were studied using the B3PW91 and TD-B3PW91 methods. The effect of the double substitution R and R' on the electronic properties of the four complexes has been investigated. Replacing the two fluorine atoms with the two methoxy groups modifies the shape of the UV-vis spectra and red shift the phosphorescence spectra, while the substituents on the linker R' do not induces changes in both spectra. Normal modes involved in the vibronic structure were identified and analyzed using adiabatic Hessian approaches according to the Franck-Condon approximation. The computed phosphorescence wavelengths agree with the observed ones and indicate that the fluorinated complexes exhibit a bright light blue color, while the methoxy complexes display a light spring green color.

## Introduction

Cyclometalated iridium and platinum complexes have been extensively studied in the last two decades owing principally to their applications in phosphorescent organic light-emitting diodes (OLEDs) and also in photocatalysts [1–5]. Octahedral iridium complexes, with C<sup>N</sup> bidentate ligands in particular phenylpyridine, phenylpyrazole, and acetylacetonate ligands showed a high luminescence quantum yield and short luminescent lifetime into the microsecond range at room temperature [6–9]. These remarkable properties have made these complexes highly preferable in OLED applications as phosphorescent emitters. Square planar geometry around the metal has also been widely considered due to the different coordination possibilities that can develop between the ligands and the metal in this geometry [10–13]. The easy synthesis of square planar complexes and the flexibility of their geometrical structures have allowed the use of various cyclometalating ligands such as bidentate, tridentate, or tetradentate [14–16]. In recent years, several studies have shown that Pt square planar complexes can be considered as an excellent alternative to the usual octahedral iridium complexes [17–19]. Square planar Pt complexes based on tetradentate ligands have recently been of great interest due to their rigid structures and due to their efficiency in OLED applications [20–22]. Chiheon Lee et al have synthesized and characterized a new series of four square Pt(II) complexes based on two tetradentate bipyridine ligands (pypy) linked by C(OCH<sub>3</sub>)R' group [23]. The four complexes have general formula  $[dRppy-C(OCH_3)R'-dRppy]Pt$ , with **Pt-1** (R = F, R'=methyl), **Pt-2** (R = F, R'=hexyl), **Pt-3** (R = methoxy, R'=methyl) and **Pt-4** (R = methoxy, R'=hexyl). The authors studied the effects of the substituents methyl or hexyl at the linker and the effects of the introduction of an electron-donating/withdrawing fragment (fluorine or methoxy) on the structure and the phosphorescence properties of the four complexes.

In this work, we studied geometrical structure, optical and phosphorescence properties of the four complexes using density functional theory (DFT) and time-dependent DFT (TD-DFT) methods. Our study provides detailed investigation on structural and electronic properties of both ground state and excited triplet state of the four complexes. The emission spectra were modeled using the Franck-Condon (FC) approximation taking into account the vibrational structure contributions to S<sub>0</sub>-T<sub>1</sub> transition.

## Computational details

Starting from X-ray geometries, all studied complexes were fully optimized in dichloromethane (CH<sub>2</sub>Cl<sub>2</sub>) using hybrid exchange–correlation functional B3PW91 [24–26]. We have employed LANL2DZ base set [27, 28] for all atoms augmented with *d* polarization functions on C, N, S, and O, and augmented with *f* polarization functions on Pt. The "relativistic" HayWat pseudo-potential associated with LANL2DZ basis set was used to describe the inner electron of the Pt. The solvent effects were introduced using the polarizable continuum model PCM [29, 30] implemented in Gaussian [31]. The low-lying excited states were studied using the TD-DFT method in term of natural transition orbitals (NTOs) [32]. All spectra were simulated with gaussian function (FWHM = 0.35 eV) using GaussSum GUI application [33]. S<sub>0</sub> geometries were used as starting point to optimize the first triplet excited states T<sub>1</sub> of all studied complexes by unrestricted DFT (UB3PW91) in CH<sub>2</sub>Cl<sub>2</sub> with the same basis sets cited above. Frequency calculations were performed to confirm that both S<sub>0</sub> and T<sub>1</sub> geometries of all complexes correspond to true minima on the Potential Energy Surface (PES). Phosphorescence wavelengths were calculated according to  $\Delta SCF^{vert}$  and  $\Delta SCF^{adiab}$  procedures. 0–0 wavelengths were calculated taking into account zero-point vibrational energy (ZPVE) corrections. To simulate the phosphorescence spectra, the vibrational structure contributions to the T<sub>1</sub>-S<sub>0</sub> electronic transition were studied using adiabatic

Hessian (AH) and adiabatic shift (AS) approaches according to the FC approximation. Emission spectra were plotted using VMS program [34]. All calculations were performed by Gaussian 09. We have use Avogadro-1 [35] to get isosurface orbitals and to visualizing geometric structures.

## Results and discussions

### Ground-state study

Ground state geometries ( $S_0$ ) of the four complexes were fully optimized in  $\text{CH}_2\text{Cl}_2$  using B3PW91 functional. Selected bond lengths and angles are given in Table 1 together with available experimental data (data not available for complex **Pt-3**). As the crystal structures, all optimized geometry complexes display a distorted square planar geometry around the metal (Fig. 1). As shown in Table 1, computed bond lengths and bond angles agree with experimental values. For all complexes, Pt – N bond lengths are slightly longer than Pt – C bond lengths. Pt –  $\text{N}_1$  and Pt- $\text{N}_2$  bond lengths are closes in each complex, which means that  $\text{N}_1$  and  $\text{N}_2$  coordinate similarly with Pt. Same conclusion for Pt –  $\text{C}_1$  and Pt –  $\text{C}_2$ . Replacing methyl with hexyl and/or fluorine atoms with methoxy groups does not affect Pt-ligand bonds lengths.

Table 1  
Selected optimized and experimental bond lengths (in Å) and bond angles (in °) of the four studied complexes calculated with B3PW91.

	Pt-1		Pt-2		Pt-3		Pt-4	
	B3PW91	Exp <sup>[23]</sup>	B3PW91	Exp <sup>[23]</sup>	B3PW91	B3PW91	Exp <sup>[23]</sup>	
Pt – $\text{N}_1$	2.079	2.064	2.079	2.068	2.075	2.080	2.057	
Pt – $\text{N}_2$	2.093	2.077	2.093	2.075	2.080	2.075	2.054	
Pt – $\text{C}_1$	1.988	1.995	1.988	1.987	1.989	1.988	1.980	
Pt – $\text{C}_2$	1.987	1.996	1.986	1.993	1.988	1.988	1.997	
$\text{N}_1$ – Pt- $\text{N}_2$	93.3	93.9	92.9	93.6	95.4	95.2	96.0	
$\text{N}_1$ – Pt- $\text{C}_1$	80.7	80.8	80.7	80.9	81.6	81.1	80.8	
$\text{C}_2$ – Pt- $\text{C}_1$	104.0	103.8	104.3	103.6	101.8	102.9	102.1	
$\text{C}_2$ – Pt- $\text{N}_2$	81.3	81.0	81.3	81.4	81.8	81.4	81.3	
$\text{C}_2$ – Pt- $\text{N}_1$	167.5	171.1	167.2	168.9	170.0	169.6	171.1	
$\text{C}_1$ – Pt- $\text{N}_2$	173.4	173.5	172.7	173.7	174.8	174.8	176.5	

Frontier molecular orbitals (FMOs) of the four complexes were studied using B3PW91 functional. Energy levels, energy gaps and the composition selected FMOs in term of orbital fragments are depicted in Scheme 1. Energy levels of fluorinated complexes (**Pt-1** and **Pt-2**) are lower than those of **Pt-3** and **Pt-4** containing methoxy groups instead fluorine atoms due to the electron withdrawing character of fluorine atoms. While replacing methyl with hexyl at the linker do not affect the energies and the compositions of FMOs of **Pt-1** and **Pt-3**. The five highest occupied orbitals (HOMO – H-5) of **Pt-1** and **Pt-2** are delocalized over pypy ligands and dPt orbitals with different percentages. The proportion of dPt orbitals are dominated only in H-2 orbitals in both **Pt-1** and **Pt-2**. For the complexes **Pt-3** and **Pt-4**, the two highest occupied orbitals HOMO and H-1 are delocalized only over pypy orbitals while the four orbitals H-2, H-3, H-4 and H-5 are contributed with dPt and pypy orbitals. The lowest unoccupied orbitals of the four complexes (Scheme 1) are delocalized in pypy orbitals without any contribution of dPt orbitals. Replacing methyl with hexyl at the linker don't affect the energy gaps, indeed **Pt-1** and **Pt-2** have very close energy gaps 4.02 and 4.03 eV respectively also **Pt-3** and

**Pt-4** have almost same energy gaps ( $\Delta E \approx 3.72$  eV). While, the energy gaps of the fluorinated complexes (**Pt-1** and **Pt-2**) are larger than **Pt-3** and **Pt-4** containing dimethoxy-pypy ligands.

## UV-vis absorption spectra

Singlet excited states of the four complexes were studied using B3PW91 functional in  $\text{CH}_2\text{Cl}_2$ . Absorption spectra were simulated using gaussian band shape with a fixed full width at half-minimum (FWHM) of 0.33 eV (Fig. 2). Wavelengths, oscillator strengths and character of selected  $S_0-S_n$  absorptions are reported together with experimental data in Table 2 (**Pt-1** and **Pt-3**) and Table S1 (**Pt-2** and **Pt-4**). As shown in Fig. 2, B3PW91 gives acceptable results compared to the experience and reproduces the main characteristic of the observed spectra. A comparison between **Pt-1** and **Pt-2** spectrum and between **Pt-3** and **Pt-4** spectrum, shows that the replacement of methyl group with hexyl group do not change the shape of both simulated and experimental spectra. While replacing the four fluorine atoms of **Pt-1** and **Pt-2** by four methoxy groups to get **Pt-3** and **Pt-4** affects the spectrum shapes. Indeed, **Pt-1** and **Pt-2** spectrum contain multiple bands between 250 and 400 nm unlike **Pt-3** and **Pt-4** spectrum which contain two distinctive bands. The singlet excited states of **Pt-1** and **Pt-3** reported in Table 2 are quasi similar with those of **Pt-2** and **Pt-4** respectively. For this reason, we only studied the excited states of **Pt-1** and **Pt-3** in terms of NTOs (Tables 3 and S2).  $S_0-S_1$  ( $f = 0.01$ ) and  $S_0-S_2$  ( $f = 0.06$ ) absorptions of **Pt-1** calculated at 370 and 349 nm respectively correspond to single hole-electron transition which occurs principally from dPt to pypy ligand orbitals and to intra-pypy ligands charge transfer. We can assign these absorptions to the weak band observed at 350–390 nm. The weak band simulated at the region 325–350 nm is contributed with  $S_0-S_3$  ( $f = 0.13$ ) and  $S_0-S_4$  ( $f = 0.11$ ) absorptions calculated at 321 and 314 nm.  $S_0-S_3$  contains double hole-electron transitions, the first (weight = 0.66) correspond to a mixed character MLCT/LLCT while the second (weight = 0.33) principally to LLCT transition.  $S_0-S_4$  absorption contains one hole-transition and corresponds to MLCT/ILCT character. The two absorptions  $S_0-S_3$  and  $S_0-S_4$  can be attributed to the two absorptions observed at 332 and 306 nm respectively. The intense band simulated at  $\sim 300$  nm is contributed with  $S_0-S_5$  and  $S_0-S_6$  absorptions with significant oscillator strengths  $f = 0.27$  and  $f = 0.23$  respectively.

Table 2  
Wavelengths ( $\lambda_{\text{cal}}$  and  $\lambda_{\text{exp}}$ ), oscillator strengths and the character of selected singlet excited states of **Pt-1** and **Pt-3**.

	$\lambda_{\text{cal}}$	$f$	Transition	$\lambda_{\text{exp}}^{[23]}$	Character
<b>Pt-1</b>					
S <sub>1</sub>	370	0.01	H-1→LUMO (95%)		MLCT/LLCT
S <sub>2</sub>	349	0.06	H-2→LUMO (79%)	<b>377</b>	MLCT/LLCT
S <sub>3</sub>	321	0.13	HOMO→L + 1 (52%) H-3→LUMO (31%)	<b>332</b>	MLCT/LLCT
S <sub>4</sub>	314	0.11	H-4→LUMO (78%)	<b>306</b>	LLCT
S <sub>5</sub>	285	0.27	H→L + 2 (36%) H-3→L + 1 (31%)		LLCT/MLCT
S <sub>6</sub>	279	0.23	H-3→L + 1 (45%) H-2→L + 1 (25%)	<b>273</b>	LLCT/MLCT
S <sub>7</sub>	250	0.22	H-3→L + 3 (46%) H-2→L + 3 (20%)		LLCT/MLCT
<b>Pt-3</b>					
S <sub>1</sub>	405	0.06	HOMO→LUMO (82%)	<b>421</b>	MLCT/LLCT
S <sub>2</sub>	356	0.16	H-2→LUMO (61%)	<b>356</b>	MLCT/LLCT
S <sub>3</sub>	334	0.21	H-4→LUMO (69%) HOMO→L + 1 (20%)		MLCT/LLCT
S <sub>4</sub>	309	0.22	H-4→L + 1 (15%) HOMO→L + 2 (64%)		LLCT
S <sub>5</sub>	290	0.39	H-4→L + 1 (34%) H-1→L + 3 (18%)	<b>295</b>	LLCT/MLCT
S <sub>6</sub>	281	0.14	H-4→L + 2 (10%) H-4→L + 3 (11%) H-3→L + 3 (47%)	<b>272</b>	LLCT/MLCT

NTO analyzes show that the two absorptions are composed with two hole-electron transitions, with two different proportions corresponding to MLCT/LLCT characters. The two absorptions are assigned to the most intense band observed experimentally above 270 nm. For **Pt-3**, S<sub>0</sub>-S<sub>1</sub> absorption computed at 405 nm containing one NTO pair transition correspond to a mixed character MLCT/LLCT and can be assigned to the weak band observed at ~420 nm. The band simulated at 320-350 nm is attributed principally with two absorptions S<sub>0</sub>-S<sub>2</sub> ( $f=0.16$ ) and S<sub>0</sub>-S<sub>3</sub> ( $f=0.21$ ). NTO analysis show that the two absorptions correspond to transitions from dPt and pypy ligand orbitals to pypy ligand orbitals. The two absorptions are assigned to the band observed at 330-380 nm. The two most intense absorptions S<sub>0</sub>-S<sub>4</sub> ( $f=0.22$ ) and S<sub>0</sub>-S<sub>5</sub> ( $f=0.39$ ) computed at 309 and 290 nm are assigned to the intense band observed at ~295 nm. S<sub>0</sub>-S<sub>4</sub> and S<sub>0</sub>-S<sub>5</sub> contain two hole-electron transitions, one dominant and the second minority corresponding both to MLCT/LLCT characters (Table 3).

## First triplet excited state study

The first triplet excited states  $T_1$  of the studied complexes were optimized in  $\text{CH}_2\text{Cl}_2$  using UB3PW91 functional. Frequency calculations were performed to check that  $T_1$  obtained correspond to true global minimum. A comparison between  $T_1$  of the four complexes show that introducing substituents methyl or hexyl at the linker between the two pypy ligands does not change  $T_1$  bond lengths (Table 4 and S3). While, the substituents on the two pyridine ligands (fluorine or methoxy), cause a slight modification around Pt and on intra-pypy ligand bonds. A comparative study between  $S_0$  and  $T_1$  geometries are reported in Table 4 (**Pt-1** and **Pt-3**) and in Table S3 (**Pt-2** and **Pt-4**). Only bond lengths with significant  $|T_1-S_0|$  are reported and classified in descending order. In **Pt-1** and **Pt-2**, Pt-N and Pt-C bonds of one pypy ligand are the most affected bonds around Pt. Indeed, the two pyridines of pypy become closer to Pt through N and C by 0.044 and 0.022Å respectively. Pt-N and Pt-C bond lengths between Pt and the second pypy ligand don't change significantly ( $\sim 0.003\text{Å}$ ) after  $S_0-T_1$  transition. For intra-ligand bond lengths, the most affected bonds are located in pyridine rings of one pypy ligand which shows that during  $T_1$  relaxation the electronic redistribution occurs only on this ligand (colored bonds in Fig. 1). For the methoxy complexes (**Pt-3** and **Pt-4**), Pt-N and Pt-N reducing by 0.035 and 0.034Å after  $S_0-T_1$  transition, are the most affected bonds around the metal. For ligand bond lengths, the most important deformations occur over the two pypy ligands. Visualizations of the singly occupied natural orbital (SONO) pairs of all  $T_1$  show that charge density distribution are localized in one pypy ligand for **Pt-1** and **Pt-2** and delocalized over the two pypy ligands for **Pt-3** and **Pt-4**.

Table 4  
A comparison between  $S_0$  and  $T_1$  geometries of **Pt-1** and **Pt-3** complexes. Bond length colors are depicted in Fig. 1.

Pt-1	Pt-3			Pt-1	Pt-3		
	$S_0$	$T_1$	$ T_1-S_0 $		$S_0$	$T_1$	$ T_1-S_0 $
Pt-N <sub>2</sub>	2.093	2.049	0.044	Pt-N <sub>1</sub>	2.075	2.040	0.035
Pt-C <sub>2</sub>	1.987	1.965	0.022	Pt-N <sub>2</sub>	2.080	2.046	0.034
Pt-N <sub>1</sub>	2.079	2.076	0.003	Pt-C <sub>1</sub>	1.989	1.975	0.014
Pt-C <sub>1</sub>	1.988	1.991	0.003	Pt-C <sub>2</sub>	1.988	1.976	0.012
C-C <sub>red</sub>	1.47	1.398	0.072	N-C <sub>green</sub>	1.373	1.403	0.03
N-C <sub>green</sub>	1.362	1.426	0.064	N-C <sub>green</sub>	1.375	1.403	0.028
C-C <sub>blue</sub>	1.400	1.453	0.053	C-C <sub>red</sub>	1.463	1.435	0.028
C-C <sub>yellow</sub>	1.436	1.483	0.047	C-C <sub>red</sub>	1.463	1.435	0.028
C-C <sub>orange</sub>	1.402	1.437	0.035	C-C <sub>blue</sub>	1.415	1.441	0.026
C-C <sub>black</sub>	1.396	1.428	0.032	C-C <sub>blue</sub>	1.416	1.442	0.026
N-C <sub>purple</sub>	1.319	1.293	0.026	C-C <sub>yellow</sub>	1.434	1.453	0.019
N-C <sub>brown</sub>	1.321	1.346	0.025	C-C <sub>yellow</sub>	1.434	1.452	0.018
C-C <sub>pink</sub>	1.392	1.369	0.023	C-C <sub>pink</sub>	1.391	1.408	0.017

## Phosphorescence properties

Phosphorescence spectra of the four studied complexes were modelled using AH method and superposed with experimental spectra for comparison (Fig. 3). Normal modes with frequencies low than  $150\text{ cm}^{-1}$  were cleared to get sufficient spectrum

progressions (> 95% for all complexes). Simulated phosphorescence wavelengths of most intense band of all spectra are given in Table 5 together with experimental data. Simulated phosphorescence spectra of the four complexes reproduce nicely the experimental ones. Introducing the substituent hexyl with methyl at the linker doesn't change the shape of **Pt-1** and **Pt-3** spectra. While replacing fluorine atoms with methoxy groups red shifts the phosphorescence spectra of **Pt-1** and **Pt-2**. Normal modes involved in the vibronic structure are reported in Table 6. For **Pt-1** and **Pt-2**, the most intense band simulated at 470 nm is not contributed by 0–0 transition but with the modes 118 and 115 for **Pt-1** and with 153 and 150 for **Pt-2**, which have intense stick near to 470 nm. All these modes correspond to in-plane vibrations localized in one pypy ligand assigned to the breathing of the pypy rings and to C-H bending, and are assigned to the intense band observed in **Pt-1** and **Pt-2** spectra. The shoulder simulated at ~ 500 nm is contributed by the modes  $|118^2$  and  $|118^1|115^1$  for **Pt-1** and by the modes  $|153^2$  and  $|153^1|150^1$  for **Pt-2**. Noting that  $|n^2$  corresponds to the case where the vibration mode  $n$  is at  $v = 2$  and  $|n^1|m^1$  is a combination of the vibration mode  $n$  at  $v = 1$  with the vibration mode  $m$  at  $v = 1$ . These vibration modes can be assigned to the weak band observed at 495 nm (**Pt-1**) and 500 nm (**Pt-2**). The bands simulated at 442 nm (**Pt-1**) and 444 nm (**Pt-2**) which have not been recorded experimentally, are contributed with 0–0 transition and the mode 28 (**Pt-1**) and 36 (**Pt-2**). For the methoxy complexes, the intense band simulated at 486 nm (**Pt-3**) and at 484 nm (**Pt-4**) are contributed principally with 0–0 transition. Additional modes near to 0–0 transition with non-negligible intensity contribute to this intense band, in particular modes 41 (**Pt-3**) and 72 (**Pt-4**) assigned mainly to in-plane vibrations of pypy fragment. The shoulder in 500–550 nm region of **Pt-3** and **Pt-4** spectra can be assigned to the vibrational signatures of two modes (87, 156) and (124, 135) in **Pt-3** and **Pt-4** spectra respectively (Table 6).

Table 5  
Computed and experimental phosphorescence wavelengths of the studied complexes.

	<b>Pt-1</b>		<b>Pt-2</b>		<b>Pt-3</b>		<b>Pt-4</b>	
	AH	Exp <sup>[23]</sup>	AH	Exp <sup>[23]</sup>	AH	Exp <sup>[23]</sup>	AH	Exp <sup>[23]</sup>
$\lambda$ /nm	498/470/442	495/466	500/473/444	500/466	510/486	515/494	510/484	515/490
CIE(x,y)	(0.17,0.22)	(0.15,0.26)	(0.17,0.24)	(0.17,0.29)	(0.17,0.47)	(0.16,0.46)	(0.17,0.50)	(0.20,0.47)

Phosphorescence colors of the four complexes were studied according to CIE-1931 color system. Color-calculator program was used to generate the CIE (x,y) coordinates from simulated (FC/AH) spectra and also from digitized experimental spectra for comparison (Table 6). As depicted in the CIE chromaticity diagram (Fig. 4), simulated and experimental (x,y) coordinates are located in the same color region of the horseshoes. Which mean that AH/FC method reproduces nicely the observed phosphorescence colors of all complexes. The fluorinated complexes **Pt-1** and **Pt-2** exhibit light bright blue color while the two methoxy complexes **Pt-3** and **Pt-4** exhibit light spring green color. Replacing methyl with hexyl group does not significantly change the CIE (x,y) coordinates of **Pt-1** and **Pt-3** and therefore don't affects the their phosphorescence colors.

## Conclusion

In this study, the geometrical, optical, and phosphorescence properties of the four complexes were investigated using the B3PW91 and TD-B3PW91 methods. The computed bond lengths and bond angles align with experimental data. Analysis of  $S_0$  and  $T_1$  for all complexes indicates that the introduction of methyl or hexyl substituents in the linker, as well as the replacement of fluorine atoms with methoxy groups, does not lead to significant modifications in  $S_0$  and  $T_1$  bond lengths. Furthermore, the electronic relaxation of  $T_1$  occurs principally on one pypy ligand for fluorinated complexes and over the two pypy ligands for methoxy complexes. B3PW91 provides acceptable results compared to experimental data and reproduces the main characteristics of both absorption and phosphorescence spectra. The substituents on the linker do not affect the spectra, while the replacement of fluorine atoms with methoxy groups on the pyridine ligands modifies the shape of the UV-vis spectra and induces a red shift in the phosphorescence spectra. NTO analyses show that the most intense absorptions, simulated in the 250–300 nm region, correspond to MLCT/LLCT character. Normal modes near to the 0–0 transition involved in the vibronic structure were identified and analyzed. The fluorinated complexes exhibit light bright blue color while the methoxy complexes display light spring green color. Moreover, replacing the two methyl groups with two hexyl groups doesn't affect the phosphorescent colors.

## Declarations

## Conflict of interest statement

On behalf of all authors, the corresponding author states that there is no conflict of interest.

## Author Contribution

Author contributions HM : Conceptualization, Data curation, Formal analysis, Investigation, Methodology, Resources, Software, Visualization, Writing – original draft. HB and DH : Conceptualization, Data curation, Formal analysis, Funding acquisition, Investigation, Methodology, Project administration, Resources, Software, Supervision, Validation, Visualization, Writing – original draft, Writing – review & editing. MB and FYC : Conceptualization, Data curation, Formal analysis, Methodology, Resources, Software, Validation, Visualization. AG : Conceptualization, Data curation, Formal analysis, Funding acquisition, Investigation, Methodology, Project administration, Resources, Software, Supervision, Validation, Visualization, Writing – review & editing.

## Acknowledgements

This work is part of *Projets de Recherche Formation-Universitaire* (PRFU, MESRS, Algeria) supported by the directorate general for scientific research and technological development (DGRSDT, [www.dgrsdz.dz](http://www.dgrsdz.dz)) and the thematic research agency in science and technology (ATRST, [www.atrst.dz](http://www.atrst.dz)). PRFU code: B00L01UN200120230005. All the authors thank DGRSDT.

## References

1. Yu, T.; Zhang, C.; Zhao, Y.; Guo, S.; Liu, P.; Li, W.; Fan, D. Synthesis, Crystal Structure and Photoluminescence of a Cyclometalated Iridium(III) Coumarin Complex. *J. Fluoresc.* **2013**, *23* (4), 777-783. DOI: 10.1007/s10895-013-1214-x.
2. Latouche, C.; Skouteris, D.; Palazzetti, F.; Barone, V. TD-DFT Benchmark on Inorganic Pt(II) and Ir(III) Complexes. *J. Chem. Theory Comput.* **2015**, *11* (7), 3281-3289. DOI: 10.1021/acs.jctc.5b00257.
3. Schira, R.; Latouche, C. DFT vs. TDDFT vs. TDA to simulate phosphorescence spectra of Pt- and Ir-based complexes. *Dalton Trans.* **2021**, *50* (2), 746-753. DOI: 10.1039/d0dt03614e.
4. Mezouar, H.; Brahim, H. Theoretical investigation on orange-emitting cyclometalated platinum (II) complexes containing organosilyl/organocarbon-substituted 2-(2-thienyl)pyridine ligands. *Photochem. Photobiol. Sci.* **2022**. DOI: 10.1007/s43630-022-00192-5.
5. Qiu, L.; Dong, A.; Zhang, S.; Wang, S.; Chang, Z.; Lu, Y.; Sui, Z.; Feng, L.; Chen, Q. Fluorinated phenylpyridine iridium (III) complex based on metal-organic framework as highly efficient heterogeneous photocatalysts for cross-dehydrogenative coupling reactions. *J. Mater. Sci.* **2020**, *55* (22), 9364-9373.
6. Leesakul, N.; Kullawanichaiyanan, K.; Mutić, S.; Guzsavány, V.; Nhukeyaw, T.; Ratanaphan, A.; Saithong, S.; Konno, T.; Sirimahachai, U.; Promarak, V. A photoactive iridium (III) complex with 3-methyl-2-phenyl pyridine and 1, 1-bis (diphenylphosphino) methane: Synthesis, structural characterization and cytotoxicity in breast cancer cells. *J. Coord. Chem.* **2021**, *74* (14), 2380-2394.
7. Chen, S.; Gai, X.; Liang, J.; Ye, K.; Liu, Y.; Wang, Y. Highly efficient phosphorescent organic light-emitting diodes based on novel bipolar iridium complexes with easily-tuned emission colors by adjusting fluorine substitution on phenylpyridine ligands. *Journal of Materials Chemistry C* **2021**, *9* (26), 8329-8336, 10.1039/D1TC01498F. DOI: 10.1039/d1tc01498f.
8. Han, D.; Ji, X.; Zhao, L.; Pang, C. Theoretical insight on electronic structure and photophysical properties of a series of cyclometalated iridium (III) complexes bearing the substituted phenylpyrazole with different electron-donating or electron-accepting groups. *Photochem. Photobiol. Sci.* **2021**, *20* (11), 1487-1495.
9. Liu, X.; Wu, S.; Wang, Y.; Li, Y.; Wang, R.; Yu, T.; Su, W.; Zhao, Y.; Zhang, D. Synthesis and luminescence properties of two cross-linkable Ir (III) complexes. *New J. Chem.* **2021**, *45* (40), 19154-19163.



10. Song, J.; Xiao, H.; Fang, L.; Qu, L.; Zhou, X.; Xu, Z.-X.; Yang, C.; Xiang, H. Highly Phosphorescent Planar Chirality by Bridging Two Square-Planar Platinum (II) Complexes: Chirality Induction and Circularly Polarized Luminescence. *J. Am. Chem. Soc.* **2022**.
11. Stolaroff, A.; Rio, J.; Latouche, C. Accurate computations to simulate the phosphorescence spectra of large transition complexes: simulated colors match experiment. *New J. Chem.* **2019**, *43* (30), 11903-11911. DOI: 10.1039/c9nj02388g.
12. Brahim, H. DFT/TD-DFT investigation on the UV-vis absorption and phosphorescence spectra of platinum(II) and palladium(II) complexes with Schiff-base ligands. *J. Lumin.* **2019**, *210*, 96-103. DOI: 10.1016/j.jlumin.2019.02.030.
13. Puttock, E. V.; Sturala, J.; Kistemaker, J. C.; Williams, J. G. Platinum (II) Complexes of Tridentate-Coordinating Ligands Based on Imides, Amides, and Hydrazides: Synthesis and Luminescence Properties. *Eur. J. Inorg. Chem.* **2021**, *2021* (4), 335-347.
14. Lantushenko, A. O.; Meger, Y. V.; Tverdokhle, N. M.; Yakovleva, Y. A.; Eltsov, O. S.; Evstigneev, M. P. Study of aggregation of O<sup>-</sup> N<sup>-</sup> N<sup>-</sup> O Pt (II) complexes in solution. *J. Mol. Liq.* **2021**, *334*, 116062.
15. Hruzd, M.; Le Poul, N.; Cordier, M.; Kahlal, S.; Saillard, J.-Y.; Achelle, S.; Gauthier, S.; Robin-Le Guen, F. Luminescent cyclometalated alkynylplatinum (ii) complexes with 1, 3-di (pyrimidin-2-yl) benzene ligands: synthesis, electrochemistry, photophysics and computational studies. *Dalton Trans.* **2022**, *51* (14), 5546-5560.
16. Li, X.; Hu, J.; Wu, Y.; Li, R.; Xiao, D.; Zeng, W.; Zhang, D.; Xiang, Y.; Jin, W. Tunable luminescence of cyclometalated platinum (II) derivatives based on novel pyrimidine-contained tridentate Pt (N<sup>-</sup> C<sup>-</sup> N) Cl complexes. *Dyes Pigm.* **2017**, *141*, 188-194.
17. Huh, J. S.; Sung, M. J.; Kwon, S. K.; Kim, Y. H.; Kim, J. J. Highly Efficient Deep Blue Phosphorescent OLEDs Based on Tetradentate Pt (II) Complexes Containing Adamantyl Spacer Groups. *Adv. Funct. Mater.* **2021**, *31* (23), 2100967.
18. Zhang, H.; Wang, W.; Liu, C.; Peng, Z.; Du, C.; Zhang, B. Highly phosphorescent platinum (ii) complexes supported by (2-(1 H-benzimidazole)-phenyl) diphosphine oxide ancillary ligands. *Journal of Materials Chemistry C* **2021**, *9* (30), 9627-9636.
19. Cebrián, C.; Mauro, M. Recent advances in phosphorescent platinum complexes for organic light-emitting diodes. *Beilstein J. Org. Chem.* **2018**, *14* (1), 1459-1481.
20. Li, G.; Liu, S.; Sun, Y.; Lou, W.; Yang, Y.-F.; She, Y. N-Heterocyclic carbene-based tetradentate platinum (ii) complexes for phosphorescent OLEDs with high brightness. *Journal of Materials Chemistry C* **2022**, *10* (1), 210-218.
21. Li, G.; She, Y. Tetradentate cyclometalated platinum complexes for efficient and stable organic light-emitting diodes. *Light Emitting Diode-An Outlook On the Empirical Features and Its Recent Technological Advancements* **2018**, 77-101.
22. Wu, C.; Zhang, Y.; Miao, J.; Li, K.; Zhu, W.; Yang, C. Tetradentate cyclometalated platinum complex enables high-performance near-infrared electroluminescence with excellent device stability. *Chin. Chem. Lett.* **2022**.
23. Lee, C.; Zaen, R.; Park, K.-M.; Lee, K. H.; Lee, J. Y.; Kang, Y. Blue phosphorescent platinum complexes based on tetradentate bipyridine ligands and their application to organic light-emitting diodes (OLEDs). *Organometallics* **2018**, *37* (24), 4639-4647.
24. Perdew, J. P. Density-functional approximation for the correlation energy of the inhomogeneous electron gas. *Physical Review B* **1986**, *33* (12), 8822-8824. DOI: 10.1103/physrevb.33.8822.
25. Becke, A. D. Density-functional thermochemistry. III. The role of exact exchange. *J. Chem. Phys.* **1993**, *98* (7), 5648. DOI: 10.1063/1.464913.
26. Perdew, J. P.; Burke, K.; Wang, Y. Generalized gradient approximation for the exchange-correlation hole of a many-electron system. *Physical Review B* **1996**, *54* (23), 16533-16539. DOI: 10.1103/physrevb.54.16533.
27. Hay, P. J.; Wadt, W. R. Ab initio effective core potentials for molecular calculations. Potentials for the transition metal atoms Sc to Hg. *J. Chem. Phys.* **1985**, *82* (1), 270. DOI: 10.1063/1.448799.
28. Hay, P. J.; Wadt, W. R. Ab initio effective core potentials for molecular calculations. Potentials for K to Au including the outermost core orbitals. *J. Chem. Phys.* **1985**, *82* (1), 299. DOI: 10.1063/1.448975.
29. Cancès, E.; Mennucci, B.; Tomasi, J. A new integral equation formalism for the polarizable continuum model: Theoretical background and applications to isotropic and anisotropic dielectrics. *J. Chem. Phys.* **1997**, *107* (8), 3032. DOI: 10.1063/1.474659.
30. Cossi, M.; Barone, V.; Mennucci, B.; Tomasi, J. Ab initio study of ionic solutions by a polarizable continuum dielectric model. *Chem. Phys. Lett.* **1998**, *286* (3-4), 253-260. DOI: 10.1016/s0009-2614(98)00106-7.

31. M.J. Frisch, G. W. T., H.B. Schlegel, G.E. Scuseria, M.A. Robb, J.R. Cheeseman, G. Scalmani, V. Barone, B. Mennucci, G.A. Petersson, H. Nakatsuji, M. Caricato, X. Li, H.P. Hratchian, A.F. Izmaylov, J. Bloino, G. Zheng, J.L. Sonnenberg, M. Hada, M. Ehara, K. Toyota, R. Fukuda, J. Hasegawa, M. Ishida, T. Nakajima, Y. Honda, O. Kitao, H. Nakai, T. Vreven, J.A. Montgomery Jr., J.E. Peralta, F. Ogliaro, M. Bearpark, J.J. Heyd, E. Brothers, K.N. Kudin, V.N. Staroverov, R. Kobayashi, J. Normand, K. Raghavachari, A. Rendell, J.C. Burant, S.S. Iyengar, J. Tomasi, M. Cossi, N. Rega, J.M. Millam, M. Klene, J.E. Knox, J.B. Cross, V. Bakken, C. Adamo, J. Jaramillo, R. Gomperts, R.E. Stratmann, O. Yazyev, A.J. Austin, R. Cammi, C. Pomelli, J.W. Ochterski, R.L. Martin, K. Morokuma, V.G. Zakrzewski, G.A. Voth, P. Salvador, J.J. Dannenberg, S. Dapprich, A.D. Daniels, J.B. Foresman, J.V. Ortiz, J. Cioslowski, D.J. Fox. *Gaussian 09, Gaussian, Inc., Wallingford CT 2009*.
32. Martin, R. L. Natural transition orbitals. *The Journal of Chemical Physics* **2003**, *118* (11), 4775-4777. DOI: 10.1063/1.1558471.
33. O'Boyle, N. M.; Tenderholt, A. L.; Langner, K. M. cclib: A library for package-independent computational chemistry algorithms. *J. Comput. Chem.* **2008**, *29* (5), 839-845. DOI: 10.1002/jcc.20823.
34. Licari, D.; Baiardi, A.; Biczysko, M.; Egidi, F.; Latouche, C.; Barone, V. Implementation of a graphical user interface for the virtual multifrequency spectrometer: The VMS-Draw tool. *J. Comput. Chem.* **2014**, *36* (5), 321-334. DOI: 10.1002/jcc.23785.
35. Hanwell, M. D.; Curtis, D. E.; Lonie, D. C.; Vandermeersch, T.; Zurek, E.; Hutchison, G. R. Avogadro: an advanced semantic chemical editor, visualization, and analysis platform. *J. Cheminform.* **2012**, *4* (1), 17. DOI: 10.1186/1758-2946-4-17.

## Tables

Tables 3 and 6 are available in the Supplementary Files section.

## Schemes

Scheme 1 is available in the Supplementary Files section

## Figures

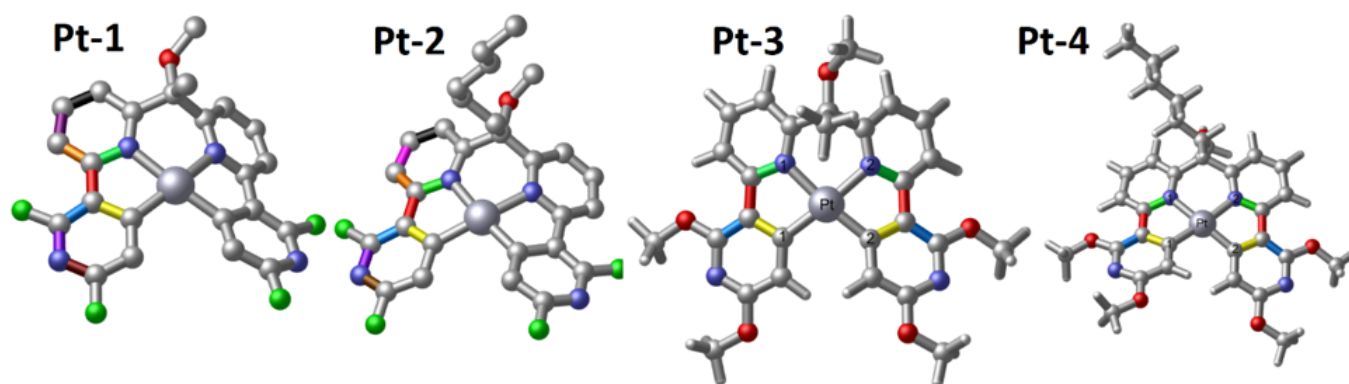


Figure 1

Geometric structures ( $S_0$ ) of the studied complexes optimized with B3PW91.

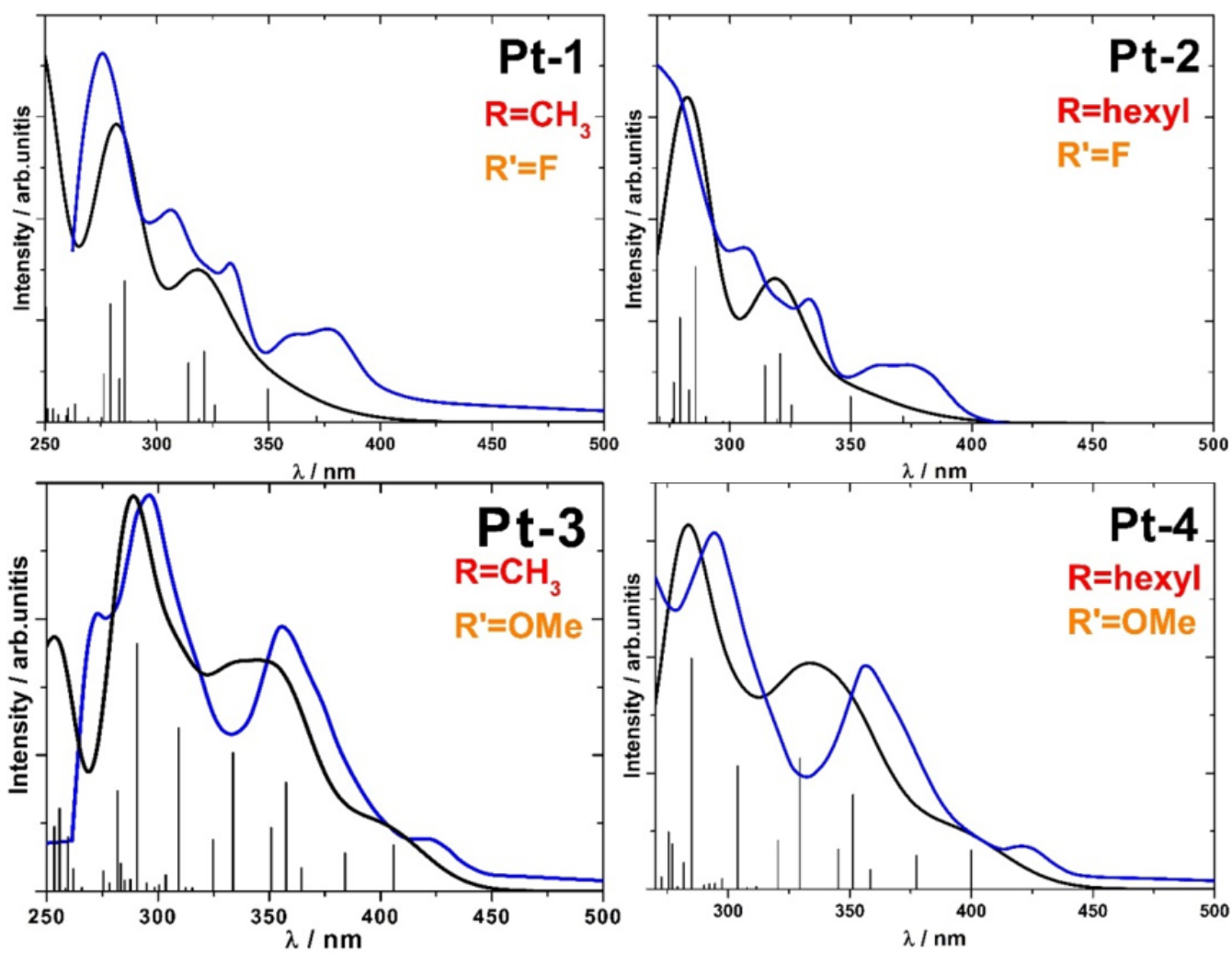


Figure 2

Experimental (blue) and simulated (black) electronic absorption spectra of the four complexes. Experimental spectra digitized from [23].

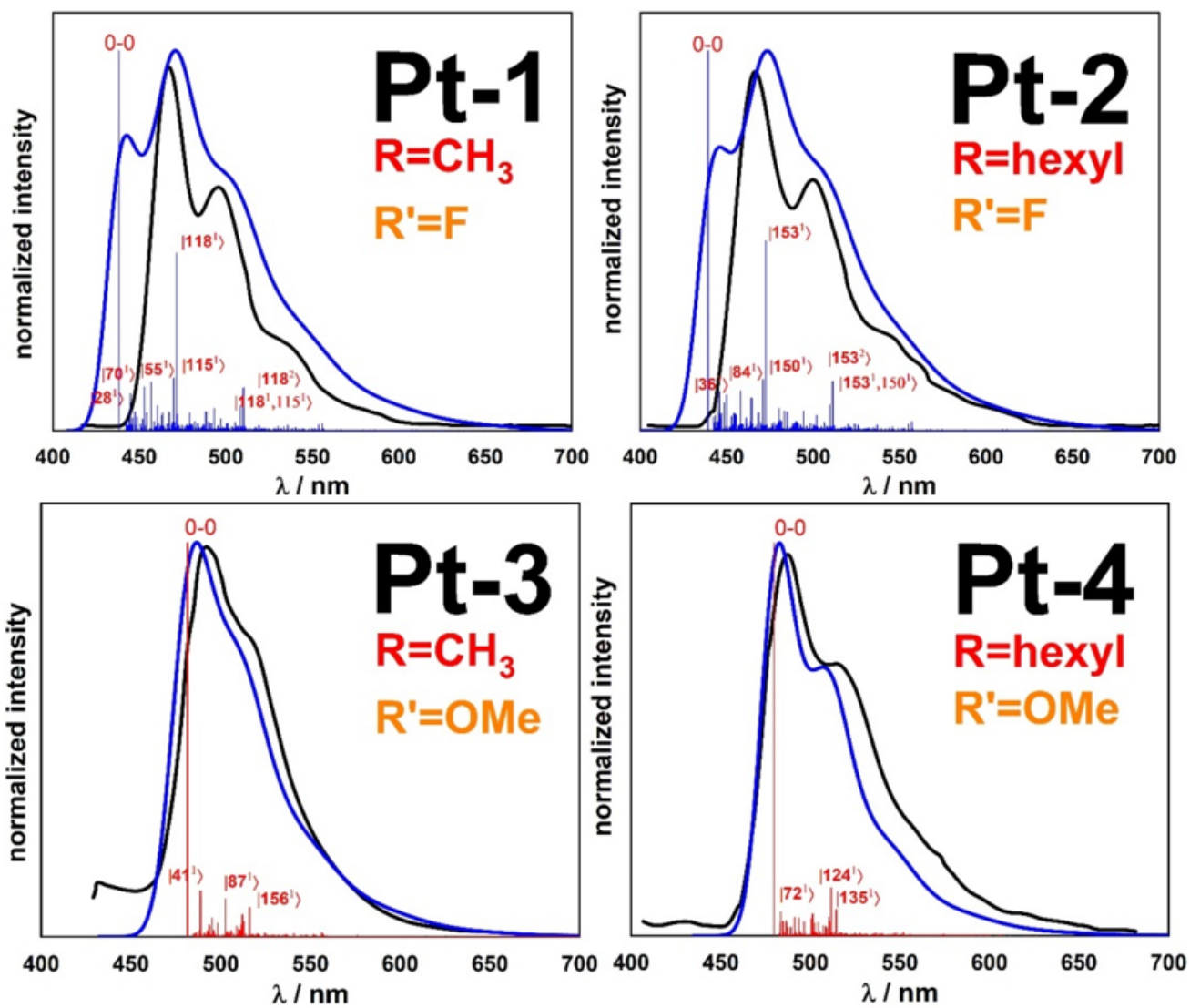
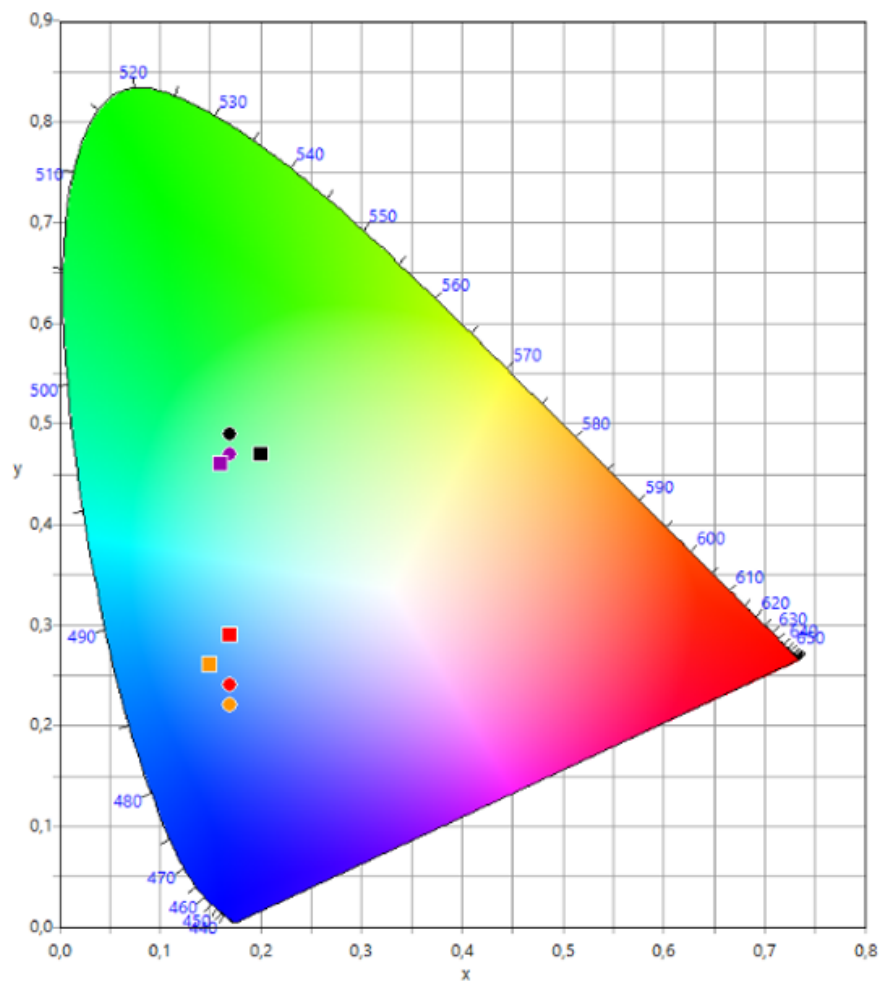


Figure 3

Simulated and experimental phosphorescence spectra of the studied complexes with normal modes involved in the vibronic structure.



**Figure 4**

CIE chromaticity diagram of **Pt-1** (orange), **Pt-2** (red), **Pt-3** (violet) and **Pt-4** (black). AH/FC coordinates in circle and exp coordinates in square (Exp<sup>[23]</sup>).

## Supplementary Files

This is a list of supplementary files associated with this preprint. Click to download.

- [Sl.docx](#)
- [Scheme1.png](#)
- [Table3and6.docx](#)